Investigating the Dynamics of Carbanion Protonation by Means of Laser Flash Electron Photoinjection from an Electrode

Jean Gamby,[1a] Philippe Hapiot,[1b] and Jean-Michel Savéant*,[1a]

Laboratoire d'Electrochimie Moléculaire, Université de Paris 7 - Denis Diderot, Case Courrier 7107, 2 place Jussieu, 75251 Paris Cedex 05, France, and Laboratoire d'Electrochimie, Synthèse et Electrosynthèse Organiques - UMR 6510, Université de Rennes 1, Campus de Beaulieu - Bat. 10C, 35042 Rennes Cedex, France

Received: April 24, 2003; In Final Form: June 23, 2003

The investigation of protonation/deprotonation at carbon is traditionally limited to molecules where acidity has been boosted by introduction of an electron-withdrawing group or by removal of an electron. These restrictions can be removed by application of the laser flash electron photoinjection technique. A thin layer of radicals is initially formed upon reduction of an appropriate substrate by the photoinjected electrons. The time-resolved current−potential responses for the reduction of the radicals thus generated are sensitive to the rate of the protonation of the ensuing carbanion by purposely added acids. The second-order rate constant may then be extracted from the half-wave potential versus time data with satisfactory accuracy in a wide range of values that extends up to the diffusion limit. The method is demonstrated with the example of diphenylmethyl and benzyl carbanions. Several observations may be derived from these first illustrating experiments. There is a large kinetic isotope effect. Proton transfer is intrinsically slow, showing that this property is not the result of the presence of an electron-withdrawing group. The intrinsic barrier is larger in the benzyl case than in the diphenylmethyl case. Unusual temperature effects (negative activation enthalpy) are observed at least in some cases, calling for systematic investigation in future studies.

Introduction

Proton transfer at carbon atoms has attracted and continues to attract considerable attention, mostly driven by attempts to explain the reasons that it appears as intrinsically slower than that for "normal" acid/base couples involving atoms such as oxygen and nitrogen.[2,3] In fact, the experimental data on which these discussions are based concern two families of rather peculiar acid/base couples. One is constituted by carbon acids that bear an electron-withdrawing group directly borne by the carbon or located in a conjugated position to it on an unsaturated substituent,[2] with particular emphasis on nitro groups as electron-withdrawing substituents.[4−6] The privileged consideration of these acids derives from the fact that the presence of an electron-withdrawing substituent makes them strong enough for the experimental determination of the rate of the deprotonation by usual bases to be achievable by means of standard methods such as stopped-flow techniques. It is conceivable that the ideas put forward to rationalize the slowness of proton transfer in these cases [7] be related to the very fact that these acids bear an electron-withdrawing substituent. A second manner of making the carbon acid strong enough to be amenable to measuring the deprotonation rate constant is to remove an electron from a p orbital. The cation radicals thus generated are indeed much stronger acids than their closed-shell precursors. In several cases the deprotonation kinetics is slow enough for conventional monitoring of reactant or product concentrations to be achieved.[8,9,10] Direct (cyclic voltammetry, potential step chronoamperometry)[11−13] and indirect (redox catalysis)[13b−d] electrochemical techniques, where the deprotonation step is coupled with the electron transfer step that produces the cation radical, have been widely used for the determination of the deprotonation rate constant. Laser flash photolysis has been used for the same purpose[13b−d,14a,15] as well as pulse radiolysis,[14b] albeit more rarely. Here too, the fact that cation radicals are dealt with may well restrict the interpretation rationalizing the observed protonation/deprotonation reactivity data[16] to this particular class of carbon acids.

It would thus be worth extending the accessibility of proton transfer kinetics to carbon acid/base systems in which the acid form is not activated by introduction of an electron-withdrawing group or removal of an electron. We propose to apply laser flash electron photoinjection techniques to this purpose. The principle of the method that allows one to relate time-resolved photocurrent−potential responses to the protonation rate of the carbanion of interest is depicted below, taking as an example the reaction of the diphenylmethyl anion with water in *N*,*N*-dimethylformamide (DMF). The determination of the deuterium/hydrogen kinetic effect on the same system will then be described. Still with water as the acid and DMF as the solvent, the benzyl anion will serve as a second example. Protonation of the diphenylmethyl anion by 2-thionaphthol will illustrate the application of the method to a very fast reaction, close to the diffusion limit. The effect of temperature will be investigated for two examples. In one case, the reaction of the diphenylmethyl anion with acetic acid, a normal behavior is observed, while the reaction with trifluoroacetic acid is abnormal in the sense that it gives rise to a negative activation energy.

The aim of this article is thus twofold: (i) to describe the methodology for accessing proton-transfer kinetics in carbon acid/base systems in which the acid form is not activated; (ii)

* To whom correspondence should be addressed. E-mail: saveant@paris7.jussieu.fr.

10.1021/jp035108q CCC: $25.00
Published on Web 08/22/2003

SCHEME 1: Reactions Involved in an Electron Photoinjection Experiment Where a Carbanion, R^-, Is Formed from the Reduction of a Radical, R, Generated from a Precursor, RX, by Means of Photoinjected Electrons

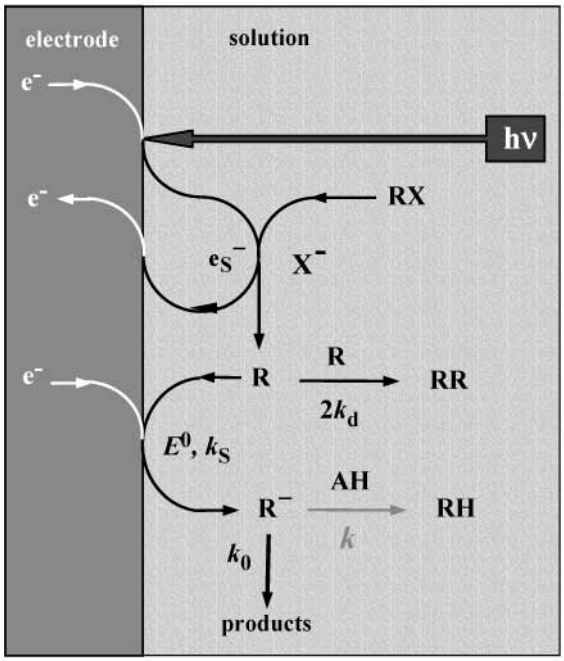

to report important preliminary findings concerning the proton-transfer reactivity in such systems.

Principle of the Method

The method consists of generating the carbanion of interest, R^-, by electrochemical reduction of the corresponding radical, $R^\bullet$, itself produced from the reductive cleavage of a precursor, RX, by electrons injected upon shining a light pulse on the electrode surface (Scheme 1). RX is selected so as to undergo a rapid bond cleavage after, or concerted with, electron transfer.[17] The reason that the reduction of RX is effected by photoinjected electrons, rather than by electrons from the electrode in a standard electrochemical reaction, derives from the observation that the reduction of the ensuing R radicals is easier than the reduction of RX in most cases.[18−20] An ECE-type mechanism would then be followed, preventing the investigation of the $R^\bullet/R^-$ couple. Instead, in a photoinjection experiment,[21] electrons are ejected from the electrode upon irradiation by a UV laser flash. After quick thermalization and solvation, the electrons are quenched by the substrate RX, thus producing the radical R. Thanks to the energy brought in by the laser pulse, the generation of the very reducing solvated electrons, and hence the production of the $R^\bullet$ radicals, occurs whether the electrode potential is set or not at a value where the radical is reduced into R^-. The reduction of $R^\bullet$ into R^- may therefore be triggered at will by changing the dc potential applied to the electrode, thus opening an opportunity to investigate the $R^\bullet + e^- \Leftrightarrow R^-$ reaction and all the reactions in which R and R^- are involved. Previous applications of the method have focused on determining the redox properties of the $R^\bullet/R^-$,[21g,i] while our present goal is the assessment of the protonation rate constant of carbanions by an acid. The first step of the procedure consists of measuring the transient photopotential, V_{ph}, triggered by application of the laser pulse in the framework of the electronic setup pictured in Figure 1.

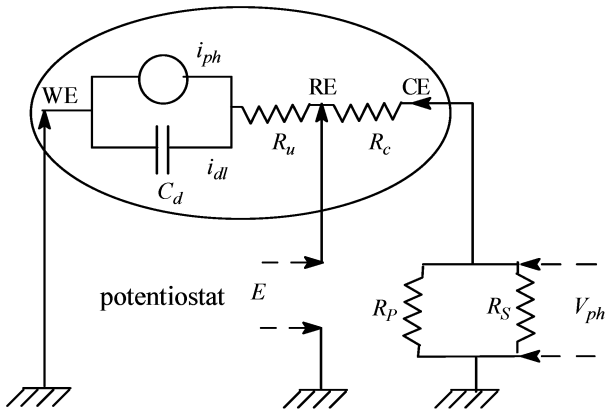

Figure 1. Equivalent circuit for the cell and instrument: WE, RE, and CE, working, reference, and counter electrodes, respectively; i_{ph}, photocurrent; i_{dl}, double layer charging current; C_d, double layer differential capacitance; R_c, R_u, cell compensated (by the potentiostat) and uncompensated resistances, respectively; R_S, sampling resistance; R_P, potentiostat resistance; E, potential difference imposed by the potentiostat between the reference and working electrodes; V_{ph}, photopotential as measured across the sampling resistor.

The photocharge is then obtained from

$$Q = \int_0^t i_{ph}\, d\eta = C_d V_{ph}\left[1 + (R_u + R_c)\frac{R_S + R_P}{R_S R_P}\right] + \frac{R_S + R_P}{R_S R_P}\int_0^t V_{ph}\, d\eta$$

with the various notations being defined in the caption of Figure 1.

The laser pulse duration is typically of the order of a few 10^{-8} s, and the light intensity is typically of the order of 20−200 kW/cm^2 (thus avoiding heating by the laser pulse[21a,d,f]). Under these conditions the photopotential does not exceed a few millivolts and does not perturb significantly the dc potential, E, imposed to the electrode by means of the potentiostat. The available time window thus ranges from $\sim 10^{-6}$ to $\sim 10^{-3}$ s. Thus, shortly after the end of the laser pulse, a thin layer of radicals has built up at the electrode surface. It is of the order of 30−100 Å thick, with surface concentration about 10^{-13} mol/cm^2. Typical variations of the photoinjected charge with the electrode dc potential, E, are as shown in Figure 2a. The fact that the variation of Q with E takes the form of a $^5/_2$-power law,[21c,d,f]

$$Q = A(E_{thr} - E)^{5/2}$$

(E_{thr} is the threshold potential and A a coefficient proportional to the photon flux) suggests recasting the $Q-E$ data as shown in Figure 2b as a $Q^{2/5}$ versus E plot, which then exhibits two converging linear asymptotes, $[Q_{foot}(E)]^{2/5} = [Q^\circ(E)]^{2/5}$ and $[Q_{plateau}(E)]^{2/5} = [2Q^\circ(E)]^{2/5}$. Their intersection provides the value of the threshold potential. $Q^\circ(E)$ is the photoinjected charge corresponding to the amount of radicals initially formed, Γ° ($\Gamma^\circ = Q^\circ(E)/F$). $2Q^\circ(E)$ is the photoinjected charge when the dc potential is negative enough for all the radicals to be reduced. The photoinjected charge thus passes from $Q^\circ(E)$ to $2Q^\circ(E)$ in the potential range where the radical is reduced. The next step is logically the construction of a radical "polarogram", defined as (Figure 2c)

$$1 + n(E) = \frac{Q(E)}{Q^\circ(E)}$$

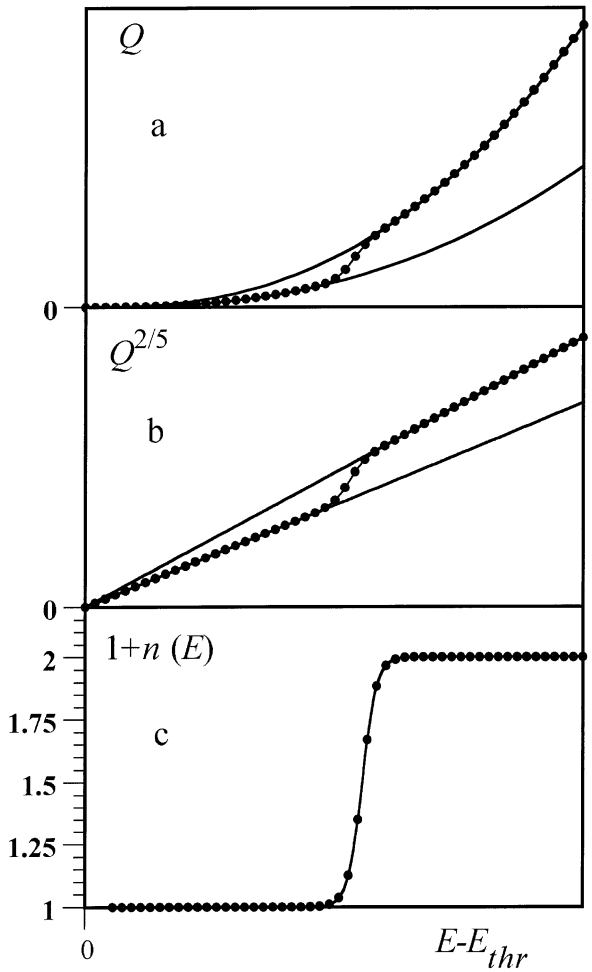

Figure 2. Variation of the photoinjected charge, *Q*, with the dc electrode potential, *E*, (a) and extraction of the apparent number of electrons (b and c).

It may happen though that the ratio between the foot and the plateau of the polarogram is somewhat smaller than 2, owing to some scavenging of the solvated electrons by impurities or by the solvent itself, as appears in blank experiments where RX has not been introduced in the solution. In such cases, the polarogram may be derived from

$$n(E) = \frac{Q(E) - Q_{\text{foot}}(E)}{Q_{\text{plateau}}(E) - Q_{\text{foot}}(E)}$$

Once the radical polarogram has been obtained, its characteristic of most interest for our purpose is the half-wave potential, insofar as its location depends on the rate of protonation of the carbanion.

Extraction of the Protonation Rate Constant from the Variations of the Half-Wave Potential with Time and Proton Donor Concentration

Reaction of Diphenylmethyl Anions with Water. Figure 3a and b shows typical radical polarograms derived according to the above procedure from photoinjection experiments carried out in the presence of diphenylmethyl chloride. In Figure 3a, no acid was added to the solution. We observe a shift of the half-wave potential, $E_{1/2}$, toward negative values, as the measurement time is decreased. This is a reflection of the irreversibility of the system caused by the electron-transfer reaction and/or the reaction of the carbanion with acidic

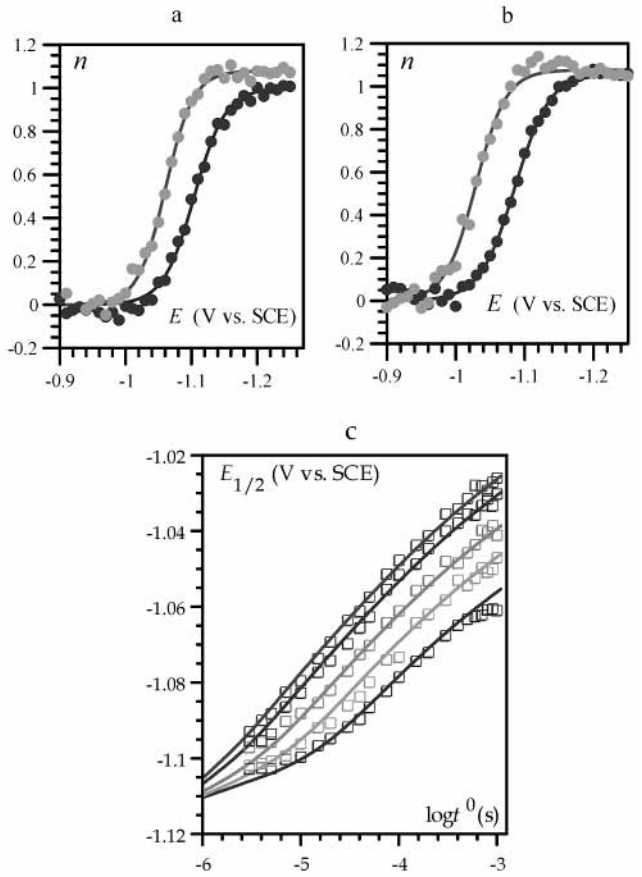

Figure 3. Reaction of diphenylmethyl anions with water in DMF + 0.1 M Et_4NClO_4 at 22 °C. (a and b) Radical polarograms at two different measurement times (full circles, 7 μs; shaded circles, 500 μs) in the absence (a) and presence of 0.52 M H_2O (b) at the diphenylmethyl chloride concentration 30 mM. (c) Variations of the half-wave potential with time for increasing concentrations of water added, from bottom to top: 0, 0.077, 0.228, 0.519, 0.764 M. Full lines: simulation for each water concentration (see text and Table 1).

impurities (e.g. water) and/or the solvent itself. Upon addition of water, the polarograms shift toward positive values, thus manifesting the interference of the protonation of the carbanion by added water, while a negative shift upon decreasing the measurement time is still observed. Figure 3c shows the result of a more systematic investigation of the variation of the half-wave potential with the measurement time, *t*, and the amount of water added. To extract the rate of the protonation reaction from the raw data in Figure 3c, all the reactions concerning $R^{\bullet}$ and R^- (Scheme 1) should be taken into account in the reaction−diffusion process involving each of the two species. In dimensionless terms, the reaction−diffusion problem may be formulated as

$$\frac{\partial a}{\partial \tau} = \frac{\partial^2 a}{\partial y^2} - \lambda_d a^2 \quad (1)$$

$$\frac{\partial b}{\partial \tau} = \frac{\partial^2 b}{\partial y^2} - \lambda b \quad (2)$$

after introduction of normalized time and space variables,

$$\tau = \frac{t}{t^\circ} \quad \text{and} \quad y = \frac{x}{\sqrt{Dt^\circ}}$$

(t°, measurement time; *D*, diffusion coefficient; *x*, distance to

the electrode, assumed to be planar) of the normalized concentrations,

$$a(y,\tau) = \frac{\sqrt{Dt^\circ}}{\Gamma^\circ}[R^\bullet] \quad \text{and} \quad b(y,\tau) = \frac{\sqrt{Dt^\circ}}{\Gamma^\circ}[R^-]$$

(Γ°, surface concentration of radicals generated at time $t = 0$).

The kinetic terms in the above two dimensionless linear diffusion Fick's law partial derivative equations pertain to the two homogeneous reactions involved. One is the dimerization of the R radicals and is characterized by the dimensionless parameter

$$\lambda_d = 2k_d\Gamma^\circ\sqrt{\frac{t^\circ}{D}} \tag{3}$$

The other concerns the quenching of the carbanions R^- both by the reaction medium (first-order rate constant, k_0) and the added acid, AH (second-order rate constant, k). The ensuing dimensionless parameter is

$$\lambda = kt^\circ = (k_0 + k_{AH}[AH])t^\circ \tag{4}$$

The above partial derivative equations are completed by the following set of initial and boundary conditions.

The initial conditions,

$$a(y,0) = \delta(y) \quad \text{and} \quad b(y,0) = 0$$

state that the initial "spatial pulse" of generated radicals may be depicted by a Dirac function of space and that there is no carbanion present at time zero.

The boundary conditions in the bulk of the solution,

$$a(\infty,\tau) = 0 \quad \text{and} \quad b(\infty,\tau) = 0$$

express the absence of radicals and carbanions, while, at the surface of the electrode, conservation of the fluxes of $R^\bullet$ and R^- leads to

$$\left(\frac{\partial a}{\partial y}\right)_{y=0} = -\left(\frac{\partial b}{\partial y}\right)_{y=0} = \psi$$

The rate law of the quasi-reversible electron-transfer reaction is in dimensionless terms

$$\psi = \Lambda \exp(\alpha\xi)[a(0,\tau) - b(0,\tau)\exp(-\xi)]$$

where

$$\xi = -\frac{F}{RT}(E - E^\circ) \quad \text{and} \quad \psi = \frac{it^\circ}{FS\Gamma^\circ}$$

are dimensionless expressions of the potential and current, respectively (E is the dc potential imposed to the electrode, E° is the standard potential of the $R^\bullet/R^-$ couple, and S is the electrode surface area). In this expression of the electron-transfer rate law, α is the transfer coefficient and Λ, the dimensionless rate parameter, is defined as

$$\Lambda = k_S\sqrt{\frac{t^\circ}{D}} \tag{5}$$

In view of its nonlinear character, the partial derivative equation system with the accompanying initial and boundary conditions is solved numerically by means of a finite difference procedure (see Supporting Information). The polarogram is finally obtained from the integration of the current function thus obtained,

$$n(\xi) = \int_0^\tau \psi(\eta)\, d\eta$$

and, therefore, the dimensionless half-wave potential, $\xi_{1/2}$. One polarogram, and, therefore, one value of $\xi_{1/2}$, is obtained for each value of the normalized time, τ. At the measurement time, t°, $\tau = 1$ is related to the experimental half-wave potential by

$$\xi_{1/2}(\tau{=}1) = -\frac{F}{RT}(E_{1/2} - E^\circ) \tag{6}$$

In the most general case, $\xi_{1/2}(\tau{=}1)$ depends on three dimensionless parameters, namely, λ_d, λ, and Λ. The next step consists of fitting the experimental data displayed as $E_{1/2}$ versus log t° curves, as, for example, in Figure 3c, with the computed $\xi_{1/2}(\tau{=}1)$ theoretical curves. This amounts, in the most general case, to adjusting the values of the following four experimental parameters: E°, through eq 6 that relates the dimensionless and the experimental half-wave potential; $k_d/\sqrt{D}$, since, in eq 3, Γ° and t° are known; $k_0 + k[AH]$, as seen in eq 4 that defines λ; and $k_S/\sqrt{D}$, from eq 5 defining Λ.

Since this four-parameter fitting is cumbersome and somewhat uncertain, it is worth considering limiting situations where the system depends on a lesser number of parameters. It is noted in this connection that, in the absence of added water, the $E_{1/2}$ versus log t° curves exhibit an inflection point that disappears upon adding water in larger and larger amounts. The total disappearance of the inflection point, corresponding to the mathematical condition $\lambda \rightarrow \infty$ (eq 4), reflects the achievement of "pure kinetic" conditions.[22] The photocurrent response may then be analyzed as follow. Because λ is large, eq 2 simplifies to

$$\frac{\partial^2 b}{\partial y^2} - \lambda b = 0$$

which expresses the establishment of a steady state resulting from the compensation of the diffusion of B and its reaction with the reaction medium and the added acid. After integration,

$$(b)_{y=0} = \frac{\psi}{\sqrt{\lambda}}$$

After introduction of

$$\tau' = \lambda_d{}^2\tau, \quad y' = \lambda_d y, \quad a' = \frac{a}{\lambda_d}, \quad \psi' = \frac{\psi}{\lambda_d{}^2}$$

this limiting situation may thus be entirely characterized by the following set of equations

$$\frac{\partial a'}{\partial \tau'} = \frac{\partial^2 a'}{\partial y'^2} - a'$$

$$a'(y',0) = \delta(y'), \quad a'(\infty,\tau') = 0$$

$$a'(0,\tau') = \psi' \exp(-\xi')$$

with

$$\exp(-\xi') = \frac{\lambda_d}{\sqrt{\lambda}}\exp(-\xi) + \frac{\lambda_d}{\Lambda}\exp(-\alpha\xi) \tag{7}$$

and

$$\psi' = \left(\frac{\partial a'}{\partial y'}\right)_{y'=0}, \quad n = \int_0^{\tau'} \psi'(\eta)\, d\eta$$

The numerical calculation of the above system, again according to a finite difference method, leads to a single $\xi_{1/2}'$ versus log τ' working curve (Figure 4a) that may be used to fit all experimental data corresponding to this limiting situation, asymptotically reached upon adding more and more acid to the solution. The treatment of the experimental data recalled in Figure 4b is as follows.

We introduce as *X*-axis

$$\log \lambda_d = \frac{1}{2}\log t^0 + \log\left(\frac{2k_d}{\sqrt{D}}\Gamma^\circ\right)$$

not only for the theoretical curves but also for the $E_{1/2}-\log t^\circ$ experimental curve. In the latter case, the fitting of the experimental data by a theoretical curve along the *X*-axis will thus lead to the assignment of a value to the parameter $2k_d/\sqrt{D}$, knowing that $\Gamma^\circ = 0.614 \times 10^{-13}$ mol cm^{-2}

$$\frac{2k_d}{\sqrt{D}} = 8.54 \times 10^{14}\ \text{mol}^{-1}\ \text{cm}^2\ \text{s}^{-1/2} \qquad (8)$$

The *Y*-axis is modified by introduction of the potential variable,

$$\xi^* = \xi + \frac{1}{2(1-\alpha)}\ln\left(\frac{\lambda}{\Lambda^2}\right) = -\frac{F}{RT}\left[E - \left\{E^\circ + \frac{RT}{2(1-\alpha)F}\ln\left[\frac{k}{\left(\frac{k_S}{\sqrt{D}}\right)^2}\right]\right\}\right]$$

not only for the theoretical curves but also for the $E_{1/2}-\log t^\circ$ experimental curve. Equation 7 thus becomes

$$\exp(-\xi') = \sqrt{\sigma}[\exp(-\xi^*) + \exp(-\alpha\xi^*)] \qquad (9)$$

with

$$\sigma = \lambda_d{}^2\frac{\lambda^{\alpha/1-\alpha}}{\Lambda^{2/1-\alpha}} = \left(\frac{2k_d}{\sqrt{D}}\Gamma^\circ\right)^2\frac{k^{\alpha/1-\alpha}}{\left(\frac{k_S}{\sqrt{D}}\right)^{2/1-\alpha}}$$

A series of theoretical curves $-\xi^*_{1/2}(\tau{=}1)/\ln 10$ versus log λ_d, built from the combination of Figure 4a and eq 9, are shown in Figure 4c for various values of the parameter σ. Fitting of the experimental data thus leads to the value

$$\sigma = \left(\frac{2k_d}{\sqrt{D}<}\Gamma^\circ\right)^2\frac{k^{\alpha/1-\alpha}}{\left(\frac{k_S}{\sqrt{D}}\right)^{2/1-\alpha}} = 8.8 \times 10^{-5} \qquad (10)$$

and

$$E^\circ + \frac{RT}{2(1-\alpha)F}\ln\left[\frac{k}{\left(\frac{k_S}{\sqrt{D}}\right)^2}\right] = -1.149\ \text{V vs SCE} \qquad (11)$$

We may thus start the simulation of the whole set of $E_{1/2}-\log t^\circ$ data (Figure 3c), taking into account three relationships between the four experimental parameters obtained by

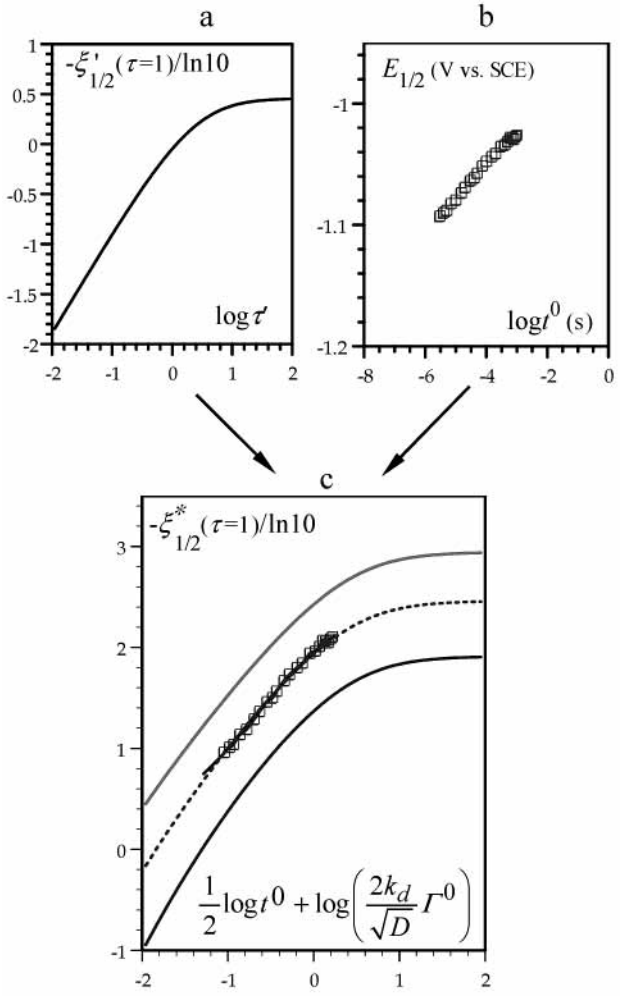

Figure 4. Reaction of diphenylmethyl anions with water in DMF + 0.1 M Et_4NClO_4 at 22 °C. Data processing under pure kinetic conditions. (a) the working curve $-\xi_{1/2}'(\tau = 1)/\ln 10$ versus log λ_d with $\log \lambda_d = {}^1/_2 \log t^\circ + \log((2k_d/\sqrt{D})\Gamma^\circ)$. (b) Experimental values of the half-wave potential at the highest water concentration. (c) Treatment (see text) of the experimental data (□): log $\sigma = -3$ (solid curve), -5 (shaded curve), -4.06 (dotted curve); straight line, general case fitting.

combination of eqs 8, 10, and 11.

$$\frac{2k_d}{\sqrt{D}} = 8.54 \times 10^{14}\ \text{mol}^{-1}\ \text{cm}^2\ \text{s}^{-1/2} \qquad (12)$$

$$\frac{k^{\alpha/1-\alpha}}{\left(\frac{k_S}{\sqrt{D}}\right)^{2/1-\alpha}} = 3.2 \times 10^{-8}\ \text{s} \qquad (13)$$

$$E^\circ + \frac{RT}{2F}\ln(k) = -0.930\ \text{V vs SCE} \qquad (14)$$

In other words, it just remains to separate E° and k in the last relationship. The best accuracy in this connection is expected when the system is far from the pure kinetic conditions, that is, when no water is added to the solution and the $E_{1/2}-\log t^\circ$ experimental curve exhibits an inflection point. Thus, in the finite difference resolution of the set of partial derivative equations, boundary and initial conditions in the general case, performed for each value of t°, $\lambda_d = (2k_d\Gamma^\circ/\sqrt{D})\sqrt{t^\circ}$, are known from $\Gamma^\circ = 0.614 \times 10^{-13}$ mol cm^{-2} and from eq 12. The next step consists, after selection of a provisional value of

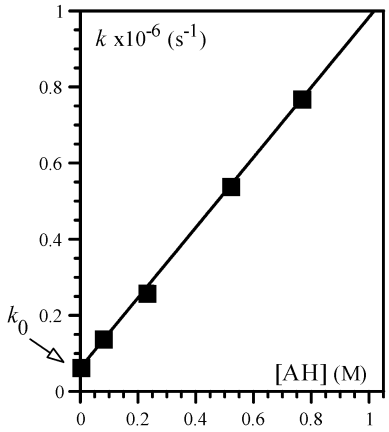

Figure 5. Reaction of diphenylmethyl anions with water in DMF + 0.1 M Et_4NClO_4 at 22 °C. Pseudo-first-order rate constant as a function of water concentration.

k, of inputting the corresponding $\lambda = kt°$ into the numerical calculation. We also need to input $\Lambda = (k_S/\sqrt{D})\sqrt{t°}$, which may be obtained from eq 13 for each particular value of $t°$, once the provisional value of k has been selected. In this derivation a is taken as equal to 0.5, in view of the fact that, as will be checked later on, the half-wave potentials are all close to the standard potential. The fitting is completed by the derivation of a value of $E°$ from eq 13, once the provisional value of k has been selected. The same procedure is applied for increasing amounts of water added (Figure 3c). The solid lines running through the data are the result of the simulation. We also note that at the highest concentration of water the pure kinetic (solid) and the general case (dotted) simulations lead to coincident lines, thus providing a self-consistency test of the whole procedure. As expected, the pseudo-first-order rate constant k is a linear function of the concentration of water (Figure 5), thus leading to the values of k_0 and k_{AH} listed in Table 1.

The difference in pK_a values between water (31.5) and diphenylmethane (32.4) in DMF[24] is only 1 unit. Assuming a Marcus-type quadratic activation/driving force relationship, the value $k°_{AH} = 10^{5.5}$ M^{-1} s^{-1} is found for the standard protonation/deprotonation rate constant (rate constant at zero driving force), thus establishing the fact that proton transfer in the diphenylmethane/diphenylmethyl anion system is intrinsically slow.

Reaction of Benzyl Anions with Water. This is an interesting second test of the extraction procedure, since we expect the kinetic competition between the electron transfer and the protonation reaction to be more in favor of electron transfer as the rate determining step, both because the electron-transfer standard rate constant is anticipated to be smaller in the benzyl case and because the protonation rate constant is anticipated to be higher (because the negative charge is more concentrated in the benzyl case than in the diphenylmethyl case). The half-wave potential−measurement time data points, obtained from the polarograms, as in the diphenylmethyl case, are shown in Figure 6a. The pure kinetic treatment may again be applied to the data points obtained at the highest water concentration. The results, displayed in Figure 7, show that the same parameters as in the diphenylmethyl case may thus be obtained. Their values are listed in Table 1. The comparison between the diphenylmethyl and the benzyl cases (Figure 7) shows that the parameter σ is, as expected, much smaller in the second case than in the first ($\log \sigma = 0.67$ against -4.06). The next step is the general case simulation of the whole set of data displayed in Figure 6a,

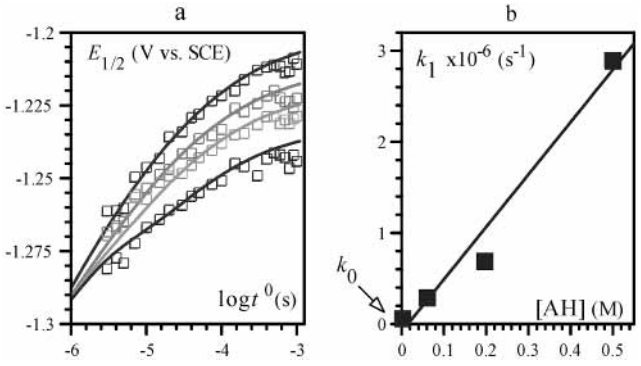

Figure 6. Reaction of benzyl anions with water in DMF + 0.1 M Et_4NClO_4 at 22 °C. (a) Variations of the half-wave potential with time for increasing concentrations of water added, from bottom to top: 0, 0.058, 0.194, 0.498 M. Full lines: simulation for each water concentration (see text and Table 1). (b) Pseudo-first-order rate constant as a function of water concentration.

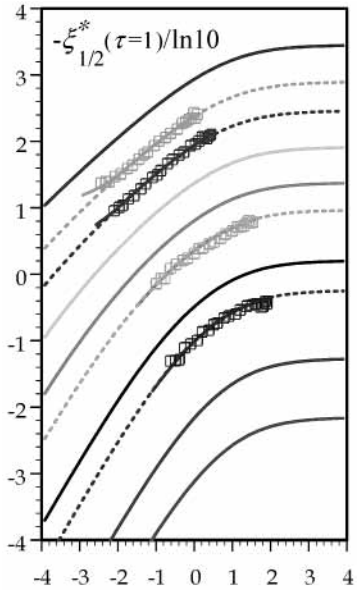

Figure 7. Pure kinetic treatment (see text) of the experimental data. Boxes are experimental data for, from top to bottom, diphenylmethyl + 0.79 M D_2O at 22 °C, diphenylmethyl + 0.765 M H_2O at 22 °C, diphenylmethyl + 0.35×10^{-3} M 2-thionaphthol at 53 °C, and benzyl + 0.498 M H_2O at 22 °C. Dotted lines are pure kinetic fittings with, from top to bottom, $\log \sigma = -4.91$, -4.06, -1.27, and -0.67. Solid lines through the boxes are general case fittings. Solid curves are theoretical pure kinetic condition curves for, from bottom to top, $\log \sigma = 3$, 2, 0, -2, and -6.

leading to the linear plot in Figure 6b, from which the protonation rate constant is finally extracted (Table 1).

The protonation rate constant is quite significantly larger than that with the diphenylmethyl carbanion. However, this is mostly due to the fact that, because the pK_a of toluene is higher (39.5),[24] the driving force is stronger (8 pK_a units). Still assuming a Marcus-type quadratic activation/driving force relationship, $k°_{AH} = 10^{3.2}$ M^{-1} s^{-1}, pointing to the conclusion that the toluene/benzyl anion system is intrinsically slower than the diphenylmethane/diphenylmethyl anion system.

Example of Fast Protonation, Close to the Diffusion Limit: Reaction of Diphenylmethyl Anions with 2-Thionaphthol

The reaction of diphenylmethyl anions with 2-thionaphthol offers an opportunity to test the electron photoinjection method

TABLE 1: Characteristic Constants Used in the General Case and Pure Kinetic Treatments of the $E_{1/2}$ − log $t°$ Data

AH	pK_a	temp (°C)	$\Gamma^0 \times 10^{13}$ (mol cm^{-2})	$2k_d/\sqrt{D} \times 10^{-14}$ (mol^{-1} cm^2 s$^{-1/2}$)	$-E°$ (V vs SCE)c	$k_S/\sqrt{D} \times 10^{-3}$ (s$^{-1/2}$)	$k^0 \times 10^{-4}$ (s^{-1})	$k_{AH} \times 10^{-8}$ (M^{-1}s^{-1})
				Diphenylmethyl Anion (pK_a = 32.4)[23a]				
H_2O	31.52[a,d,e]	22	0.61	8.5	1.102	2.2	6.8	0.0098
D_2O		22	0.52	8.5	1.117	2.2	8.1	0.0021
2-thionaphthol	11.15 [23a]	53	0.72	25	1.101	1.4	24.6	180
CH_3CO_2H	13.3 [23b]	−15.0	0.61	2.8	1.101	2.8	15.2	0.61
		1.0	0.61	4.7	1.105	2.8	10.7	0.92
		16.0	0.55	10	1.105	1.6	7.95	1.35
		44.0	0.47	21	1.098	1.6	11.5	2.01
		58.0	0.49	37	1.101	1.14	12.6	2.31
CF_3CO_2H	4.8 [23d]	−15.0	1.07	2.8	1.110	2.8	23.1	21.1
		1.0	1.07	6.3	1.115	2.8	4.94	20.1
		22.0	0.43	6.6	1.104	2.2	7.9	10.8
		44.0	1.17	4.4	1.108	1.14	1.05	10.0
				Benzyl Anion (pK_a = 39.5)[23a]				
H_2O	31.5	22	0.65	45	1.250	0.42	2.1	0.058

Γ^0: initial surface concentration of radicals, D: diffusion coefficient, k_d: dimerization rate constant, E^0: standard potential, k^0: rate constant of the reaction of the carbanion with the reaction medium, k_{AH}: protonation rate constant.

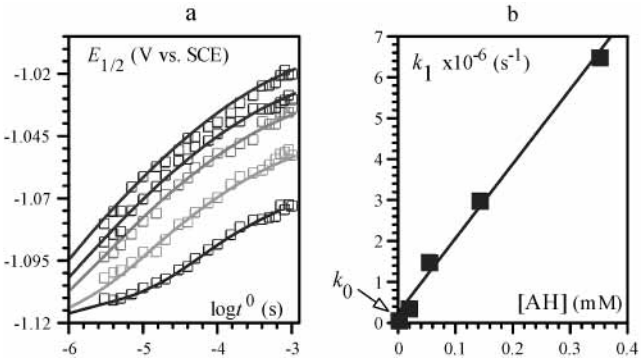

Figure 8. Reaction of diphenylmethyl anions with 2-thionaphthol in DMF + 0.1 M Et_4NClO_4 at 53 °C. (a) Variations of the half-wave potential with time for increasing concentrations of 2-thionaphthol added, from bottom to top: 0, 0.016, 0.0479, 0.127, 0.285 mM. Full lines: general case simulation for each 2-thionaphthol concentration (see text and Table 1). (b) Pseudo-first-order rate constant as a function of 2-thionaphthol concentration.

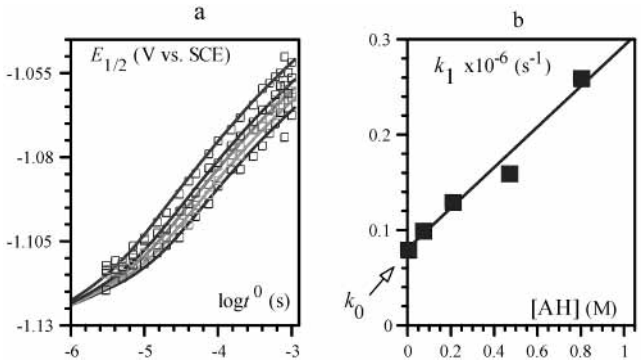

Figure 9. Reaction of diphenylmethyl anions with heavy water in DMF + 0.1 M Et_4NClO_4 at 22 °C. (a) Variations of the half-wave potential with time for increasing concentrations of water added, from bottom to top: 0, 0.068, 0.205, 0.460, 0.790 M. Full lines: simulation for each heavy water concentration (see text and Table 1). (b) Pseudo-first-order rate constant as a function of heavy water concentration.

in the case of a very fast protonation reaction, close to the diffusion limit. In this case, smaller concentrations of acid (Figure 8a) are used than those of the preceding acids in view of the expected increase of the protonation rate constant. The pure kinetic treatment is first applied to the data obtained at the highest thionaphthol concentration, showing (Figure 7) that this analysis is perfectly tractable despite the high protonation rate constant. The results of the general case analysis are shown in Figure 8a, and, for the highest acid concentration, in Figure 7 (where it is seen once again that the two analyses are coincident under these conditions). The linear variation of the ensuing pseudo-first-order rate constant of the reaction is represented in Figure 8b, leading to a second-order rate constant (Table 1) which is indeed close to the diffusion limit.

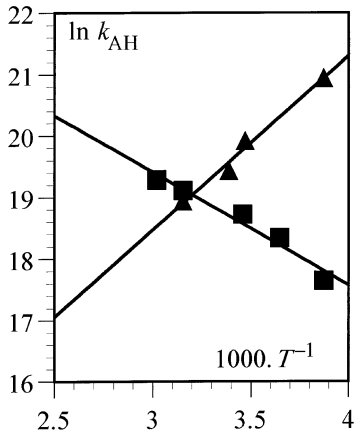

Figure 10. Arrhenius plots for the reactions of diphenylmethyl anions with acetic and trifluoroacetic acids in DMF + 0.1 M Et_4NClO_4.

TABLE 2: Activation Enthalpies and Entropies[a]

AH	$\Delta H^‡$ (eV)	$\Delta S^‡$ (meV/K)
CH_3CO_2H	0.134	−0.464
CF_3CO_2H	−0.099	−1.068

[a] $\ln(k_{AH}) - \ln(kT/h) = -\Delta H^{\#}/RT + \Delta S^{\#}/R$.

Kinetic Isotope Effect: Reaction of Diphenylmethyl Anions with Light and Heavy Water

Is it possible to detect a kinetic isotope effect? is the next question we address by comparing the reactions of the diphenylmethyl anion with light and heavy water. Starting from the $E_{1/2}$−log $t°$ data (Figure 9a), we first apply the pure kinetic treatment to the highest D_2O concentration (Figure 7) to obtain, as before, the constants that will serve in the general case treatment. The latter, applied at all D_2O concentrations (solid lines in Figure 9a), leads to the results displayed in Figure 9b, from which the second-order rate constant is derived (Table 1). A large kinetic isotope effect is thus found, $k(H_2O)/k(D_2O)$ = 4.3, pointing to proton tunneling through the activation barrier.

Normal and Abnormal Temperature Effects: Reaction of Diphenylmethyl Anions with Acetic Acid and Trifluoroacetic Acid.

Similar experiments were carried out with acetic and trifluoroacetic acid, for which the driving force is larger than those in the preceding examples (Table 1). Using the same pure kinetic and general case treatments, the protonation rate constant was investigated as a function of temperature (Table 1). Arrhenius plots were thus obtained for the two acids (Figure 10). It is interesting to note that, while acetic acid exhibits a normal temperature dependence of the protonation rate constant, with a positive activation enthalpy, trifluoroacetic acid shows a reverse behavior indicative of a negative activation enthalpy (the activation enthalpies, $\Delta H^{\ddagger}$, and entropies, $\Delta S^{\ddagger}$, are listed in Table 2).

Conclusions

Two kinds of conclusions emerge from the above discussion. The first pertains to methodology: the various examples that have been analyzed show that the laser pulse electron photoinjection technique can be applied successfully to the determination of the protonation rate constant of carbanions over ranges of values that extend up to the diffusion limit. A satisfactory accuracy on protonation rate constants, of the order of ±15%, is revealed by repeating the same experiment. It should be emphasized in this connection that small drifts in the reference electrode potential, as has been observed, do not alter the accuracy of the protonation rate constant, insofar as it remains stable during the limited time required for a series of experiments where the acid is progressively added to the solution.

A series of interesting observations concerning proton-transfer reactivity to these nonactivated systems may be derived from this first series of experiments. One is that a large kinetic isotope effect (4−5) is observed, raising the question of proton tunneling. Another is that proton transfer appears as intrinsically slow, showing that this feature is not a specific feature of carbon acids bearing an electron-withdrawing group or of cation radicals. It is also worth noting that the intrinsic barrier is larger in the benzyl case than in the diphenylmethyl case. The finding of an unusual temperature effect (negative activation enthalpy) in the reaction of diphenylmethyl anions with trifluoroacetic acid, while a normal behavior is observed with acetic acid, points to the necessity of a systematic investigation of this factor in future studies aiming at a more complete description of the reaction dynamics.

Experimental Section

Chemicals. Diphenylmethyl chloride (Aldrich, 98%) and benzyl chloride (Fluka puriss., 99.5%) were used without further purification. 2-Thionaphthol (Aldrich, 99%), acetic acid (Aldrich, 99.7%), trifluoroacetic acid (Aldrich, 99.7%), and the solvent (*N*,*N*-dimethylformamide, Fluka puriss., 99.8%, 0.01% H_2O) were used as received. Tetraethylammonium perchlorate (Fluka purum, 98%) was recrystallized from a 2−1 ethanol−ethyl acetate mixture.

Instrumentation and Procedures for Electron Photoinjection Experiments. The instrument (Figure 11) is composed of three main parts: the electrochemical cell equipped with three electrodes; an excimer laser delivering a short light pulse onto the working electrode; and the electronic setup that imposes the dc potential of the working electrode and allows the recording and integration of the transient photopotential. The whole system is triggered and controlled by a personal computer.

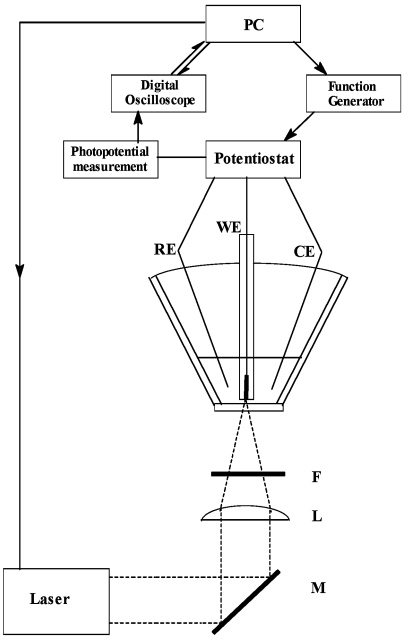

Figure 11. Instrumental setup: WE, RE, CE, working, reference, and counter electrodes, respectively; M, semitransparent mirror; L, lens; F, filter.

The potentiostat and photopotential measuring device were as described in ref 21i. The sampling resistance R_S was set equal to 100 kW in all experiments. The function generator and the digital oscilloscope were Schlumberger 4431 and Tektronix TDS 430A instruments, respectively.

The working electrode is a 0.5 mm diameter gold disk, frequently polished with diamond pastes, rinsed with acetone, and ultrasonicated in methylene chloride. The counter electrode is a platinum wire. The reference electrode is an aqueous saturated calomel electrode. Its potential is checked against the ferrocene−ferricenium couple (E° = 0.450 V vs SCE at 295 K) at the end of each series of experiments. All potentials given in the text are thus referred to the same aqueous SCE. The cell is equipped with a double jacket allowing thermostatization at a chosen temperature (a 30 min waiting time before each series of experiments at the selected temperature allows the cell and the reference electrode to stabilize). The bottom of the cell is a quartz window allowing the passage of the light beam, and the tip of the working electrode is positioned 1 mm above the window. To limit the electrical interferences, the full setup is placed inside a Faraday cage. The substrate concentration was typically in the 10−30 mM range.

The excimer laser was a Compex 100 (Lambda Physik) filled with a XeCl mixture (wavelength, 308 nm; pulse duration, 20 ns; pulse stability, ±5%). The laser beam is directed toward the cell by semitransparent mirrors and focused onto the surface of the electrode so as to cover a slightly larger area. Series of filters made with Pyrex plates are used to attenuate the beam as to obtain an energy of ∼100 μJ on the electrode surface. At the 308 nm wavelength, the substrates used in this work have no significant absorption of light.

The electrode dc potential is varied incrementally, each 5 mV, so as to cover a potential range of ±200 mV around the half-wave potential. After each of a series of 5−10 laser shots, the photopotential is sampled in the digital oscilloscope at 22 preselected times from 3 μs to 1 ms along a logarithmic incrementation. The resulting photopotential−time curves are averaged, and the averaged curve is transferred to the PC. The same cycle of operations is repeated at each value of the dc

potential, and the whole set of data, stored in the PC, is treated so as to display one polarogram for each preselected time. From this photopolarogram, the $E_{1/2}$ is directly measured by the computer (detection of the inflection point in the S-shaped polarogram), and its variation is plotted as a function of the preselected time. This operation is repeated for several concentrations of added acid to derive the protonation rate constant. In the activation investigations, this full series of experiments is completely and independently repeated for each temperature. This procedure allows cancellation of the reference electrode due to the temperature changes on the relative variation of the $E_{1/2}$ with the time and acid concentration variations (only the relative variation of the $E_{1/2}$ with the experimental parameters is required for the extraction of the protonation rate constant at each temperature).

Supporting Information Available: Finite difference procedure used to numerically solve the partial derivative equation system in the case of second-order self-reactions. This material is available free of charge via the Internet at http://pubs.acs.org.

References and Notes

(1) (a) Université de Paris 7. (b) Université de Rennes 1.

(2) (a) Bernasconi, C. F. *Acc. Chem. Res.* **1987**, *20*, 301. (b) Bernasconi, C. F. *Adv. Phys. Org. Chem.* **1992**, *27*, 119. (c) Bernasconi, C. F. *Acc. Chem. Res.* **1992**, *25*, 9. (d) Bernasconi, C. F.; Ali, M.; Gunter, J. C. *J. Am. Chem. Soc.* **2003**, *125*, 151.

(3) Anne, A.; Fraoua, S.; Hapiot, P.; Moiroux, J.; Savéant, J.-M. *J. Am. Chem. Soc.* **1995**, *117*, 7412.

(4) (a) Fukuyama, M.; Flanagan, P. W. K.; Williams, F. T.; Frainer, L.; Miller, S. A.; Schechter, H. *J. Am. Chem. Soc.* **1970**, *92*, 4689. (b) Bordwell, F. G.; Boyle, W. J., Jr. *J. Am. Chem. Soc.* **1972**, *94*, 3907. (c) Bordwell, F. G.; Bartmess, J. E.; Hautala, J. A. *J. Org. Chem.* **1978**, *43*, 3107. (d) Kresge, A. J. *Can. J. Chem.* **1975**, *52*, 1897. (e) Keeffe, J. R.; Munderloh, N. H. *J. Chem. Soc., Chem. Commun.* **1974**, 17. (f) Keeffe, J. R.; Morey, J.; Palmer, C. A.; Lee, J. *J. Am. Chem. Soc.* **1979**, *101*, 1295. (g) Cox, B. G.; Gibson, A. *J. Chem. Soc., Chem. Commun.* **1974**, 638. (h) Wilson, J. C.; Källsson, I.; Saunders, W. H., Jr. *J. Am. Chem. Soc.* **1980**, *102*, 4780. (i) Amin, M.; Saunders, W. H., Jr. *J. Phys. Org. Chem.* **1993**, *6*, 393. (j) Wilson, J. C.; Källsson, I.; Saunders, W. H., Jr. *J. Am. Chem. Soc.* **1980**, *102*, 4780. (k) Amin, M.; Saunders, W. H., Jr. *J. Phys. Org. Chem.* **1993**, *6*, 393.

(5) (a) Bernasconi, C. F.; Kliner, D. A. V.; Mullin, A. S.; Ni, J.-X. *J. Org. Chem.* **1988**, *53*, 3342. (b) Albery, W. J.; Bernasconi, C. F.; Kresge, A. J. *J. Phys. Org. Chem.* **1988**, *1*, 29. (c) Gandler, J. R.; Bernasconi, C. F. *J. Am. Chem. Soc.* **1992**, *114*, 631. (d) Bernasconi, C. F.; Wiersema, D.; Stronach, M. W. *J. Org. Chem.* **1993**, *58*, 217. (e) Bernasconi, C. F.; Ni, J.-X. *J. Org. Chem.* **1994**, *59*, 4910. (f) Bernasconi, C. F.; Panda, M.; Stronach, M. W. *J. Am. Chem. Soc.* **1995**, *117*, 9206. (g) Bernasconi, C. F.; Montanez, R. L. *J. Org. Chem.* **1997**, *62*, 8162. (h) Bernasconi, C. F.; Kittredge, K. W. *J. Org. Chem.* **1998**, *63*, 1994. (i) Bernasconi, C. F.; Wenzel, P. J.; Keeffe, J. R.; Gronert, S. *J. Am. Chem. Soc.* **1997**, *119*, 4008.

(6) (a) Farrell, P. G.; Fogel, P.; Chatrousse, A. P.; Lelièvre, J.; Terrier, F. *J. Chem. Soc., Perkin Trans. 2* **1985**, 51. (b) Fogel, P.; Farrell, P. G.; Lelièvre, J.; Chatrousse, A. P.; Terrier, F. *J. Chem. Soc., Perkin Trans. 2* **1985**, 711. (c) Terrier, F.; Lelièvre, J.; Chatrousse, A. P.; Farrell, P. G. *J. Chem. Soc., Perkin Trans. 2* **1985**, 1479. (d) Lelièvre, J.; Farrell, P. G.; Terrier, F. *J. Chem. Soc., Perkin Trans. 2* **1986**, 333. (e) Farrell, P. G.; Terrier, F.; Xie, H. Q.; Boubaker, T. *J. Org. Chem.* **1990**, *55*, 2546. (f) Terrier, F.; Xie, H. Q.; Farrell, P. G. *J. Org. Chem.* **1990**, *55*, 2610. (g) Terrier, F.; Xie, H. Q.; Lelièvre, J.; Boubaker, T.; Farrell, P. G. *J. Chem. Soc., Perkin Trans. 2* **1990**, 1899. (h) Terrier, F.; Croisat, D.; Chatrousse, A. P.; Ponet, M. J.; Hallé, J. C.; Jacob, G. *J. Org. Chem.* **1992**, *57*, 3684. (i) Terrier, F.; Lan, X.; Farrell, P. G.; Moskowitz, D. *J. Chem. Soc., Perkin Trans. 2* **1992**, 1259. (j) Terrier, F.; Boubaker, T.; Xia, L.; Farrell, P. G. *J. Org. Chem.* **1992**, *57*, 3924. (k) Moutiers, G.; El Fahid, B.; Collot, A.-G.; Terrier, F. *J. Chem. Soc., Perkin Trans. 2* **1996**, 49. (l) Moutiers, G.; Thuet, V.; Terrier, F. *J. Chem. Soc., Perkin Trans. 2* **1997**, 1479. (m) Moutiers, G.; Reignieux, A.; Terrier, F. *J. Chem. Soc., Perkin Trans. 2* **1998**, 2489.

(7) See ref 2b and c and references therein.

(8) Sinha, A.; Bruice, T. C. *J. Am. Chem. Soc.* **1984**, *106*, 7291.

(9) (a) Tolbert, L. M.; Khanna, R. K. *J. Am. Chem. Soc.* **1987**, *109*, 3477. (b) Tolbert, L. M.; Khanna, R. K.; Popp, A. E.; Gelbaum, L.; Bottomley, L. A. *J. Am. Chem. Soc.* **1990**, *112*, 2373.

(10) (a) Fukuzumi, S.; Kondo, Y.; Tanaka, T. *J. Chem. Soc., Perkin Trans. 2* **1984**, 673. (b) Fukuzumi, S.; Tokuda, Y.; Kitano, T.; Okamoto, T.; Otera, J. *J. Am. Chem. Soc.* **1993**, *115*, 8960.

(11) (a) Schlesener, C. J.; Amatore, C.; Kochi, J. K. *J. Am. Chem. Soc.* **1984**, *106*, 7472. (b) Schlesener, C. J.; Amatore, C.; Kochi, J. K. *J. Phys. Chem.* **1986**, *90*, 3747. (c) Masnovi, J. M.; Sankararaman, S.; Kochi, J. K. *J. Am. Chem. Soc.* **1989**, *111*, 2263. (d) Sankararaman, S.; Perrier, S.; Kochi, J. K. *J. Am. Chem. Soc.* **1989**, *111*, 6448.

(12) (a) Reitstöen, B.; Parker, V. D. *J. Am. Chem. Soc.* **1990**, *112*, 4698. (b) Parker, V. D.; Chao, Y.; Reitstöen, B. *J. Am. Chem. Soc.* **1991**, *113*, 2336. (c) Parker, V. D.; Tilset, M. *J. Am. Chem. Soc.* **1991**, *113*, 8778.

(13) (a) Hapiot, P.; Moiroux, J.; Savéant, J.-M. *J. Am. Chem. Soc.* **1990**, *112*, 1337. (b) Anne, A.; Hapiot, P.; Moiroux, J.; Neta, P.; Savéant, J.-M. *J. Phys. Chem.* **1991**, *95*, 2370. (c) Anne, A.; Hapiot, P.; Moiroux, J.; Neta, P.; Savéant, J.-M. *J. Am. Chem. Soc.* **1992**, *114*, 4694. (d) Anne, A.; Fraoua, S.; Hapiot, P.; Moiroux, J.; Savéant, J.-M. *J. Am. Chem. Soc.* **1995**, *117*, 7412.

(14) (a) Baciocchi, E.; Del Giacco, T.; Elisei, F. *J. Am. Chem. Soc.* **1993**, *115*, 12290. (b) Bacciocchi, E.; Bietti, M.; Putignani, L.; Steenken, S. *J. Am. Chem. Soc.* **1996**, *118*, 5952.

(15) (a) Xu, W.; Mariano, P. S. *J. Am. Chem. Soc.* **1991**, *113*, 1431. (b) Xu, W.; Zhang, X.; Mariano, P. S. *J. Am. Chem. Soc.* **1991**, *113*, 8863.

(16) Anne, A.; Fraoua, S.; Grass, V.; Hapiot, P.; Moiroux, J.; Savéant, J.-M. *J. Am. Chem. Soc.* **1998**, *120*, 2951.

(17) (a) Savéant, J.-M. *Acc. Chem. Res.* **1993**, *26*, 455. (b) Savéant, J.-M. Dissociative Electron Transfer. In *Advances in Electron-Transfer Chemistry*; Mariano, P. S., Ed.; JAI Press: New York, 1994; Vol. 4, pp 53−116. (c) Savéant, J.-M. Electron transfer, bond breaking and bond formation. In *Advances in Physical Organic Chemistry*; Tidwell, T. T., Ed.; Academic Press: New York, 2000; Vol. 35, pp 117−192.

(18) (a) Wayner, D. D. M.; Griller, D. *J. Am. Chem. Soc.* **1985**, *107*, 7764. (b) Wayner, D. D. M.; McPhee, D. J.; Griller, D. *J. Am. Chem. Soc.* **1988**, *110*, 132. (c) Griller, D.; Wayner, D. D. M. *Pure Appl. Chem.* **1989**, *61*, 754. (d) Nagaoka, T.; Griller, D.; Wayner, D. D. M. *J. Phys. Chem.* **1991**, 95, 6264. (e) Wayner, D. D. M.; Houmam, A. *Acta Chem. Scand.* **1998**, *52*, 377.

(19) (a) Andrieux, C. P.; Gallardo, I.; Savéant, J.-M. *J. Am. Chem. Soc.* **1989**, *111*, 1620. (b) Andrieux, C. P.; Grzeszczuk, M.; Savéant, J.-M. *J. Am. Chem. Soc.* **1991**, *113*, 8811. (c) Andrieux, C. P.; Grzeszczuk, M.; Savéant, J.-M. *J. Electroanal. Chem.* **1991**, *318*, 369.

(20) (a); Fuhlendorf, R.; Occhialini, D.; Pedersen, S. U.; Lund, H. *Acta Chem. Scand.* **1989**, *43*, 803. (b) Lund, H.; Daasbjerg, K.; Occhialini, D.; Pedersen, S. U. *Russ. J. Electrochem.* **1995**, *31*, 865. (c) Lund, H.; Daasbjerg, K.; Lund, T.; Occhialini, D.; Pedersen, S. U. *Acta Chem. Scand.* **1997**, *51*, 135.

(21) (a) Barker, G. C.; Gardner, A. W.; Sammon, D. C. *J. Electrochem. Soc.* **1966**, *113*, 1182. (b) Brodsky, A. M.; Gurevich, Y. Y. *Zh. Eksp. Teor. Fiz.* **1968**, *54*, 213. (c) Benderskii, V. A. *J. Electroanal. Chem.* **1977**, *76*, 327. (d) Gurevich, Y. Y.; Pleskov, Y. V.; Rotenberg, Z. A. *Photoelectrochemistry*; Plenum Press: New York, 1980. (e) Konovalov, V. V.; Raitsimring, A. M.; Tsvertkov, Y. D. *Radiat. Phys. Chem.* **1988**, *32*, 623. (f) Benderskii, V. A.; Krivenko, A. G. *Russ. Chem. Rev.* **1990**, *59*, 1 and references therein. (g) Hapiot, P.; Konovalov, V. V.; Savéant, J.-M. *J. Am. Chem. Soc.* **1995**, *117*, 1428. (h) Benderskii, A. V.; Benderskii, V. A.; Krivenko, A. G. *J. Electroanal. Chem.* **1995**, *380*, 7. (i) Gonzalez, J.; Hapiot, P.; Konovalov, V. V.; Savéant, J.-M. *J. Am. Chem. Soc.* **1998**, *120*, 10171. (j) Gonzalez, J.; Hapiot, P.; Konovalov, V. V.; Savéant, J.-M. *J. Electroanal. Chem.* **1999**, *463*, 157. (k) Gamby, J.; Hapiot, P.; Savéant, J.-M. *J. Am. Chem. Soc.* **2002**, *124*, 8798.

(22) Nadjo, L.; Savéant, J.-M. *J. Electroanal. Chem.* **1973**, *48*, 113.

(23) (a) The pK_a's are either taken directly from literature values or derived from pK_a's in dimethyl sulfoxyde (DMSO) according to pK_a(DMF) = 1.5 + 0.96pK_{aDMSO}.[23b] In the case of 2-thionaphthol, the pK_a in DMSO was derived from the pK in water[23c] according to the correlation to pK_a(DMSO) = 1.08pK_a(water) − 1.6 that we have established between the literature pK_a in water and that in DMSO over a large series of phenols and thiophenols. The pK_a of diphenylmethane derived from its value in DMSO[23d,e] is 32.4. The pK_a in DMSO for the toluene/benzyl anion couple was estimated from the thermodynamic relationship between the BDE (C−H bond dissociation energy in the gas phase), the pK_a, and $E°_{A^•/A^-}$: ΔpK_a (BDE in kcal/mol, $E°$ in V). The required values were previously measured for the diphenylmethane (BDE = 81.8,[23f] pK_a = 32.25,[23f] $E°$ = −1.107 V vs SCE) and 9-methylanthracene (BDE = 81.4,[23f] pK_a = 31.1,[23f] $E°$ = −1.020 V/SCE[21i]), leading to 39.2 and 39.8, respectively, for toluene. An averaged value of 39.5 is used in this work. (b) Maran, F.; Celadon, D.; Severin, G.; Vianello, E. *J. Am. Chem. Soc.* **1991**, *113*, 9320. (c) De Maria, P.; Fini, A.; Hall, F. M. *Gazz. Chim. Ital.* **1977**, 107. (d) Bordwell, F. G. *Acc. Chem. Res.* **1988**, *21*, 456. (e) Bartness, J. E.; Scott, J. A.; McIver, R. T., Jr. *J. Am. Chem. Soc.* **1979**, *101*, 6056. (f) Bordwell, F. G.; Cheng, J.-P.; Harrelson, J. A., Jr. *J. Am. Chem. Soc.* **1988**, *110*, 1229.